IEEE Access
Multidisciplinary ⋮ Rapid Review ⋮ Open Access Journal

Received March 17, 2019, accepted March 27, 2019, date of publication March 29, 2019, date of current version June 4, 2019.

Digital Object Identifier 10.1109/ACCESS.2019.2908340

Transverse Spurious Mode Compensation for AlN Lamb Wave Resonators

JIE ZOU[1,2], (Member, IEEE), JIANSONG LIU[1], AND GONGBIN TANG[3]
[1]Skyworks Solutions, Inc., Irvine, CA 92617, USA
[2]Lambwave LLC, Irvine, CA 92620, USA
[3]Skyworks Solutions, Inc., Kadoma 571-0050, Japan

Corresponding author: Jie Zou (zoujie0726@gmail.com)

ABSTRACT Lamb wave modes with type I dispersion characteristics exhibit strong affinity toward multi transverse modes behavior above resonance frequency (f_r) in the AlN Lamb wave resonators (LWRs), especially the high-transduction-efficiency modes: S_0 and S_1 mode. For conventional interdigital transducer (IDT) design, the IDT aperture and IDT gap are the two main factors impacting the transverse mode placements and strengths, according to the wave vector analysis and finite element method (FEM) simulation. Moreover, the convex slowness curve of the Lamb wave modes propagating in AlN platelets allows the waveguiding and weak lateral leakage into busbars by the high-velocity IDT gap region. Apodization, the standard technique to suppress the transverse modes for IDT-excited resonators, suffers from drawbacks, such as additional loss and reduction of the effective coupling coefficient (k^2_{eff}). Type I Lamb wave modes in AlN show positive slope in the dispersion branch so that a border region of lower Eigen-resonance frequency is required to form piston mode structure for transverse spurious mode suppression and lateral leakage reduction. Based on dispersion calculations and 2.5D FEM simulations, we demonstrate that by designing the low-velocity border region, such as simply changing the IDT layout, the guiding can be improved and a piston mode can be obtained for the type I Lamb wave modes.

INDEX TERMS Aluminum nitride, dispersion, lamb wave, S_0 mode, S_1 mode, transverse modes, piston mode structure.

I. INTRODUCTION

Piezoelectric microelectromechanical (MEMS) resonators offer fascinating prospects for frequency selection, control, and sensing applications thanks to its small size and low resonance impedance. Among various piezo-MEMS resonators, AlN Lamb wave resonators (LWRs) recently capture attention since they enjoys both advantages of surface acoustic wave (SAW) devices and film bulk acoustic resonators (FBARs): the multi-frequency and CMOS-compatible ability [1]–[16]. For all Lamb wave modes propagating in an AlN plate, the S_0 and S_1 mode stand out for their excellent transduction efficiency [17], [17]–[24].

In general, high quality factor (Q), large k^2_{eff}, high frequency ability and spurious free are the four most desirable fundamental aspects for micro resonators to enable low-loss filters, stable oscillators and sensitive sensors. While the S_0 and S_1 Lamb wave resonators excellently address the former three, they exhibit strong affinity toward multimode behavior near the main resonance mode along with their superior transduction efficiency. The presence of the strong transverse modes across the lateral direction would hinder the accuracy and stability of oscillators and sensors, as well as hurt the performance of acoustic filters by creating severe passband ripples and potentially limiting the rejection [25]–[43].

The transverse modes show standing wave characteristics in lateral direction and has been intensively studied for SAW and FBARs [34], [44]. In LWRs, these unwanted modes are present in the passband with relatively large aperture and are due to the poor wave-guiding properties of the IDT strips [25]. Generally, the even modes have an extra half wavelength of the sinusoidal amplitude profile leading to non-vanishing coupling in the frequency response. As a contrast, the amplitudes in opposite directions equal and the electrode signal cancel out for the odd modes intrinsically. Fig. 1 shows the displacement profile in x (propagation) direction and the mode shapes for the transverse modes in AlN LWRs.

Apodization as a standard solution for transverse modes in the IDT-excited devices by varying the resonance cavity length to smooth out the effect of transverse mode on

The associate editor coordinating the review of this manuscript and approving it for publication was Yuhao Liu.

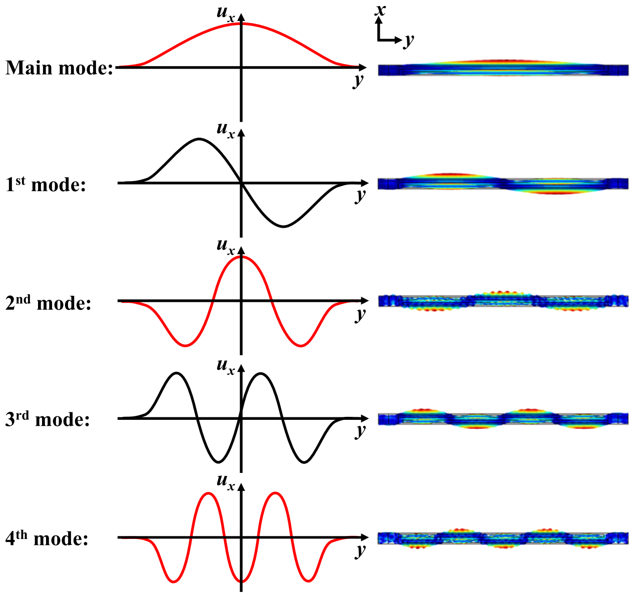

FIGURE 1. The displacement profile in x (propagation) direction u_x and the mode shapes for the transverse modes in AlN LWRs.

the electrical response, its incomplete transduction from the electrical field to main mode resonance results in substantial drawbacks such as reduction of the transduction efficiency and additional losses for both SAW filters [31] and Lamb wave resonators [45]. A better solution can be borrowed from the SAW and FBAR devices: by creating a border region with different frequency from active region according to the mode dispersion characteristic, a Piston mode structure can be obtained to cancel out the transverse wave vector in lateral direction without degrading the k_{eff}^2 or Q [25], [31]–[46], when the waveguiding and the energy confinement effects optimized in the topology.

II. DISPERSION CHARACTERISTICS OF LAMB WAVE MODES IN AlN

The phase velocity (v_p), group velocity (v_g) and the dispersion curves (f - wave number (β)) of the first six Lamb wave modes are given in Fig. 2 (a), (b) and (c). The FEM Eigen-analysis is used in for an ideal infinite plate to get the open-surface phase velocity for each mode [3] and the group velocity derived from the $v_p - \beta$ correlation. Fig. 2(a) shows that the fundamental Lamb wave modes A_0 and S_0 have weak dispersion characteristics (close to the Rayleigh mode), while the high-order Lamb wave modes are with steep dispersions. In IDT-excited device the wavelength λ ($\lambda = 2\pi/\beta$) equals 2 times IDT pitch.

As can be seen from Fig. 2(b), evidently, almost all Lamb wave modes exhibit positive v_g except the S_1 mode at $h_{AlN}/\lambda < 0.3$, where as a rare case, the energy of the S_1 Lamb wave mode would travel inside to the transducers. Accordingly, as shown in Fig. 2 (c): the S_0 mode exhibits positive slope through all wave number range, meaning the

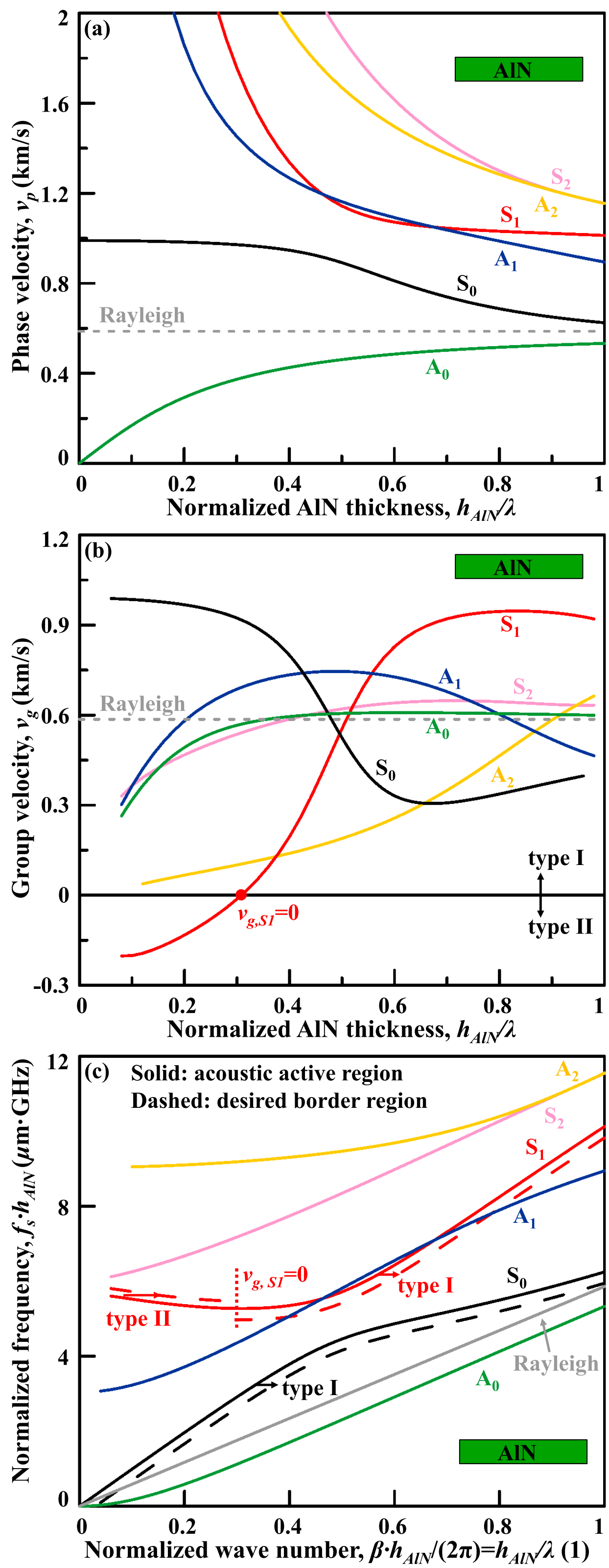

FIGURE 2. (a) Phase velocity and (b) group velocity of the first six Lamb wave modes propagating in AlN plate. (c) Dispersion curves for the first six Lamb wave modes and the desired border region eigen-frequencies for S_0 and S_1 modes.

positive v_g; the S_1 mode has a negative group velocity at $h_{AlN}/\lambda < 0.3$ and positive slope at $h_{AlN}/\lambda > 0.3$. Generally, the wave mode with positive v_g is referred to as type I dispersion, and the wave mode with negative v_g is referred to as with type II dispersion. As a result, the S_0 mode corresponds to type I dispersion through all wave number range; the type II dispersion happens to the S_1 mode at $h_{AlN}/\lambda < 0.3$ and type I dispersion occurs at $h_{AlN}/\lambda > 0.3$.

To form Piston mode structure, for resonances of type I dispersion, the frequency of the border region must be lower than that of the active area, which is the similar case for ZnO FBAR [34], solidly mounted resonators (SMRs) [37] and SAW filters (non-dispersive Rayleigh wave or SH wave has positive dispersion slope of $2\pi \bullet v_p$). On the contrary, for resonances of type II dispersion, the frequency of the border region must be higher than that of the active area, which is the case for AlN FBAR [35]. The dashed lines in Fig. 2(c) show the desired eigen-frequencies for the border region in order for the Piston mode to happen to the S_0 and S_1 modes.

Fig. 3 (a) and (b) show the simulated frequency response of the type I S_0 mode and type II S_1 mode, respectively. As expected, the transverse modes for the type I Lamb wave modes would occur above resonance frequency f_r, while for the type II Lamb wave mode the transverse modes take place below the f_r. In addition, for the LWR employing S_1 mode in the type II region, the transverse modes are not strongly excited, and some other spurious modes, such as the inter-reflection from IDT fingers due to negative group velocity, are much stronger and more of concern (Fig. 3(b)). As a result, the transverse modes and the design of Piston mode for type I Lamb wave modes are emphatically discussed herein.

III. TRANSVERSE MODES IN TYPE I LAMB WAVE MODES

The transverse modes and transverse leakage are sensitive to the lateral acoustic field distribution and controlled by the IDT designs. Similar to SAW resonators, the IDT aperture dominates the frequency locations of the transverse modes, which can be calculated by the superposition of wave vectors in longitudinal (propagation) and lateral (transverse) directions, according to the standing wave theory. The convex slowness curve of the Lamb wave modes propagating in AlN platelets allows weak lateral leakage for the LWRs with the high-velocity IDT gap regions.

A. IDT APERTURE

The standing wave nature of the transverse modes allows for direct derivation of their frequency allocations [43], [46], [47]. Intuitively, in lateral direction, the wave number is determined by the IDT aperture and transverse mode order:

$$\beta_y = \frac{\pi \cdot (n+1)}{w_a}, \tag{1}$$

where the w_a represents the active region width or aperture width and n stands for the transverse mode order. The wave number in propagation direction stays unchanged:

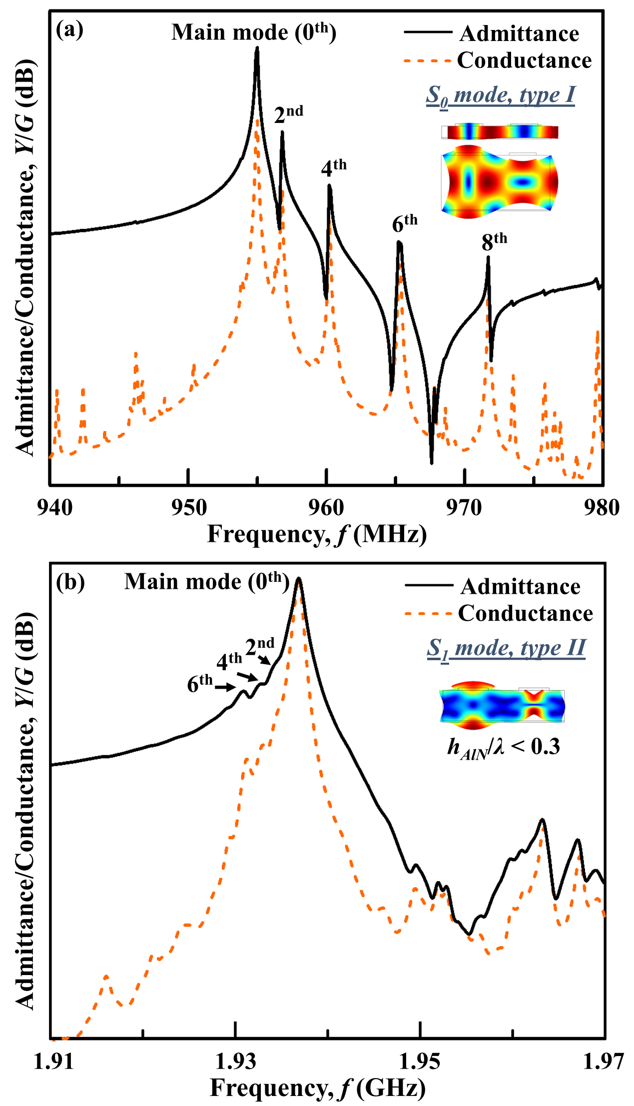

FIGURE 3. The simulated frequency response of the (a) S_0 Lamb wave mode with type I dispersion and (b) S_1 Lamb wave mode with type II dispersion when $h_{AlN}/\lambda < 0.3$.

$$\beta_x = \frac{2\pi}{\lambda}. \tag{2}$$

Using orthogonal wave vector superposition, the wave number value of the n-th transverse mode can be estimated as:

$$\beta_{n,trans} = 2\pi\sqrt{(\frac{n+1}{2\cdot w_a})^2 + (\frac{1}{\lambda})^2} = \frac{2\pi}{\lambda}\sqrt{(\frac{\lambda}{2\cdot w_a})^2(n+1)^2+1} \tag{3}$$

By the first-order Taylor expansion, the offset of wavenumber from the ideal wave propagating only in x direction is:

$$\Delta\beta = \beta_{n,trans} - \beta_x = \frac{\pi}{4\lambda}(\frac{\lambda}{w_a})^2(n+1)^2 \tag{4}$$

Substituting the group velocity definition into the first order approximation:

$$f_{n,trans} \cong f_{ideal} + \Delta\beta \bullet \frac{\partial f}{\partial \beta} = f_{ideal} + \Delta\beta \bullet v_g$$
$$\cong f_{ideal} + \frac{\pi}{4\lambda}(\frac{\lambda}{w_a})^2(n+1)^2 \bullet v_g, \quad (5)$$

where f_{ideal} corresponds to the main resonance mode when the IDT aperture is infinitely long and the wave propagates in x direction only ($\beta_{ideal} = \beta_x$, $\beta_y = 0$). It should be noted that the in the case of main mode ($n = 0$) when the IDT aperture is finite, the $f_{r,main}$ is also deviated from f_{ideal} due to the lateral displacement localization. Regardless of the sign of v_g, it can be found that the larger the order n, the farther the transverse mode away from the main mode.

Recalling $v_g > 0$ for type I dispersion and $v_g < 0$ for type II dispersion, the frequency placements of transverse modes are at opposite locations comparing to the main mode:

$$\text{Type I}: \; f_{n,trans} > f_{ideal} \approx f_{s,main}$$
$$\text{Type II}: \; f_{n,trans} < f_{ideal} \approx f_{s,main} \quad (6)$$

For the type I modes, the transverse modes appear above the f_r of main mode and locate in the upper half of the smith chart; for the type II modes the transverse spurious is at lower frequency than f_r and represents resonating circles on the southwest of smith chart. This corresponds to the transverse modes location in Fig. 3 (a) and (b).

The fundamental modes A_0 and S_0 have weak dispersion, with dispersion curve β-f close to the linear line of Rayleigh mode. For the S_0 mode, the frequencies of transverse resonances can be further approximated by ignoring the dispersion at the localized wave number β and assuming $v_p = v_g$:

$$f_{n,trans} \approx f_{ideal} + \frac{\pi}{4\lambda}(\frac{\lambda}{w_a})^2(n+1)^2 \cdot v_p$$
$$= f_{ideal}(1 + \frac{\pi}{4}(\frac{\lambda}{w_a})^2(n+1)^2). \quad (7)$$

Fig. 4(a) shows the theoretical relation between the frequency placements of the n-th transverse modes and IDT aperture by formula (7) in lines and the FEM simulated cases in dots for the type I S_0 Lamb wave mode. Fig. 4(b) depicts the FEM simulated frequency response for different normalized aperture length. Evidently, the longer the normalized active region w_a/λ, the more transverse mode will be in passband, as the wider displacement profile in transverse direction impact less on the overall wave number and thus pulls in each transverse mode to the main mode. The amplitude of each transverse resonance becomes weaker at longer aperture because of the inter energy dissipation for the closely allocated resonances [47]. Another phenomenon can be observed is for the main mode itself, that the k_{eff}^2 will degrade for too-short aperture ($w_a < 10\lambda$) as the transversal wave vector contributes to the wave vector of the main mode and diffraction takes place, which corresponds to the previous discussion on the definition of f_{ideal} and $f_{r,main}$ (for this case of type I dispersion $f_{r,main} > f_{ideal}$). In Fig. 4 (a), the FEM

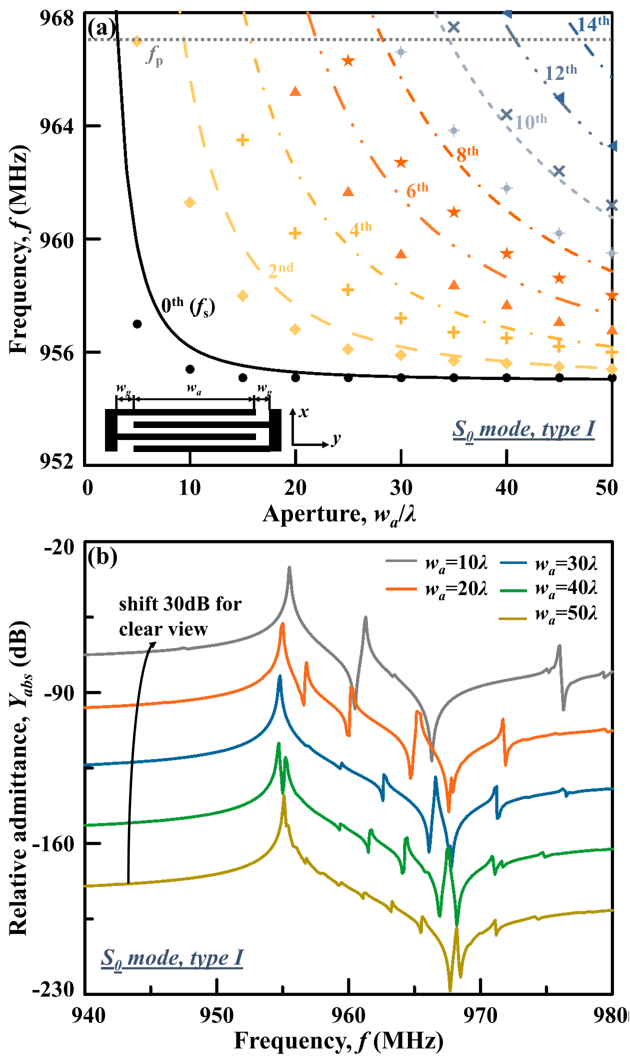

FIGURE 4. Spectra of the theoretical transverse spurious resonances as a function of aperture width w_a in lines and FEM simulated cases in dots. (b) FEM simulated frequency response for different normalized aperture lengths w_a.

simulated frequencies are lower than theoretical because the inactive regions such as busbar and gap are taken into account.

B. IDT GAP

Fig. 5 shows the slowness curves of the transducer region, gap region, and busbar region of the S_0 mode for the $h_{AlN}/\lambda = 0.1$ case as an example. Aluminum is used for IDT and the thickness is assumed to 0.08λ herein. The θ monotonically increases with frequency for the transducer, busbar, and gap regions, meaning that the S_0 Lamb wave exhibits convex slowness curve feature in all regions.

Usually for a wave with a convex slowness curve to be trapped, a faster region is required at the lateral end to guide the wave [47]. For TCSAW resonators on $SiO_2/LiNbO_3$, the faster gap region helps trapping energy, and for Quartz resonators the faster busbar region does the guiding job [31].

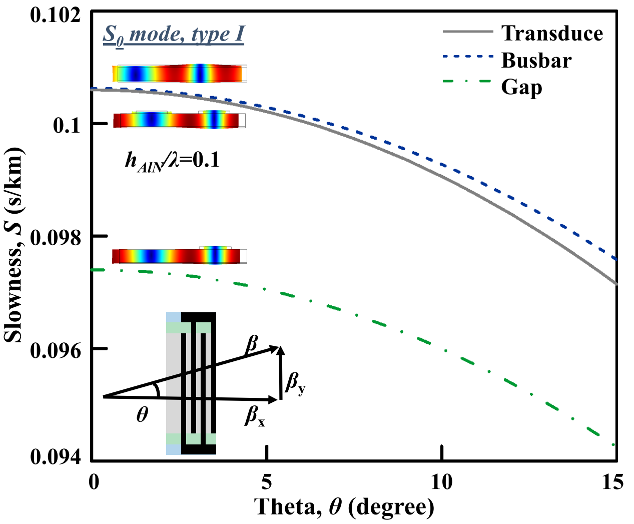

FIGURE 5. Slowness curve of the transducer region, gap region, and busbar region for the S_0 mode in AlN.

In LWRs, it can be easily found that the S_0 velocity in the busbar is lower than the S_0 velocity in the transducer caused mostly by the smaller mass loading of the transducer strips as compared to the busbar [25]. However for the S_0 mode here, the gap region exhibits too high phase velocity to make the wave guiding right at the transducer/gap interface. Also as the busbar region has phase velocity close to the transducer region, the wave guiding is actually close to the busbar/gap interface. As a result, by modifying the gap region width w_g the energy trapping would not be impact much. Unlike the TCSAW who has a larger Q for wider gap, the energy loss of S_0 Lamb wave resonator is not dependent on the gap width; rather, the gap width has direct impact on the transverse mode amplitude.

Fig. 6 depicts the simulated conductance and mechanical quality factor of S_0 resonators with different gap widths using perfectly matched layer (PML) - based FEM. In the acoustic Q calculation, an isotropic mechanical damping of 0.0003 is applied with PML on the ends of the periodic 2.5D structure, as shown in the inset of Fig. 6 (b). The Q's are automatically computed by COMSOL Multiphysics indicating the number of cycles in which total energy of the system decreases by a factor of $e^{2\pi}$ and the resistance is not considered herein.

The frequencies of the transverse modes lowered when the gap become wider, because the gap region "stretches" the active area a little bit so that the effective length of active part w_a becomes slightly larger. Unlike the SiO_2/$LiNbO_3$-based TCSAW using Rayleigh wave who also has a convex slowness curve characteristic and its high-velocity gap region provides the wave guiding, the Q's of Lamb wave aren't pronouncedly improved by wider gap when w_g/λ increases from 1 to 3 (Fig. 6(b)). However, when the fast gap region is completely taken off and $w_g = 0$, the acoustic energy of the main mode does leak to the low-velocity busbar region (inset of Fig. 6(b)) and the Q_s of the main

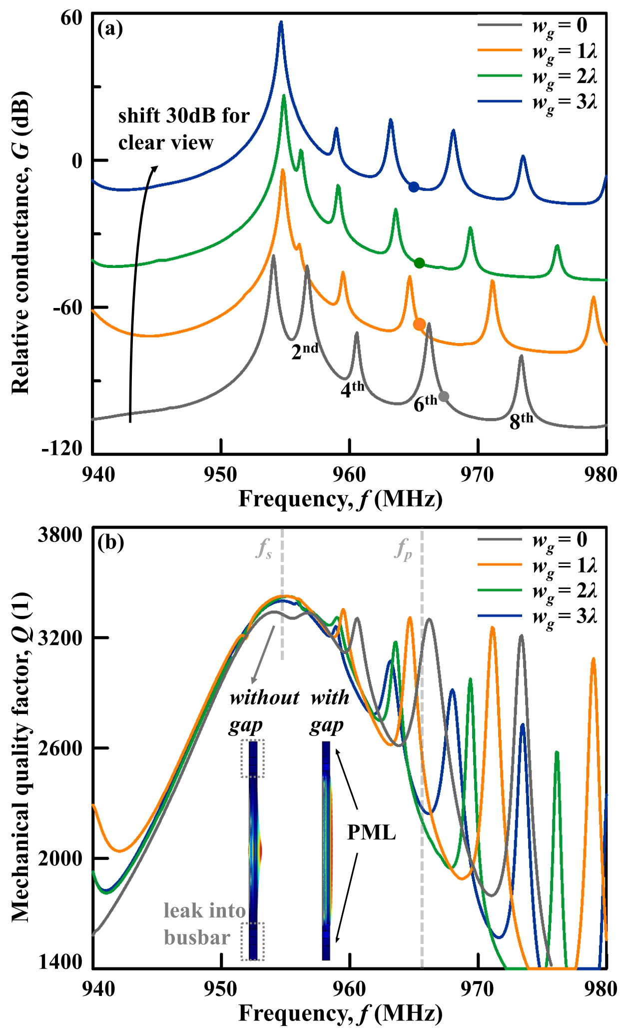

FIGURE 6. Comparison of the FEM simulated (a) conductance and (b) mechanical quality factor with different normalized gap width w_g.

mode lowered by the lateral penetration, indicating the wave guiding function provided by the fast region.

IV. PISTON MODE DESIGN FOR TYPE I LAMB WAVE MODES

A. PISTON MODE DESIGN FOR TYPE I LAMB WAVE MODES

For the type I modes, by adding a small border region with a slow velocity on the edge of the acoustic active region, a propagating mode has a zero transverse wave vector in the active aperture. The transverse wave vectors are real in the border region and imaginary on the gap region. Fig. 7 also compares the displacement profiles $u_{x,n}$ of the n^{th} transverse mode in a traditional resonator and $u_{x,n}$ of the resonator employing Piston mode. In the Piston mode structure - single mode waveguide, the effective coupling of the main mode is maximized and the displacement is at the maximum value in all active regions. In terms of the high order transverse modes, for the traditional resonator, approximately an extra half wave

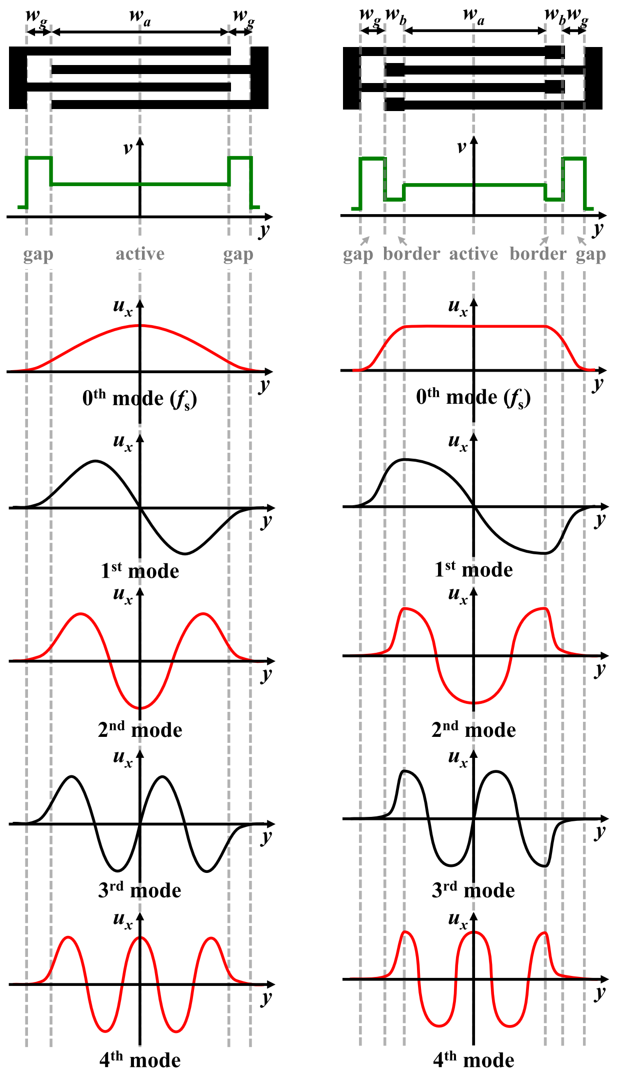

FIGURE 7. Comparison of the velocity profiles v and the displacement profiles $u_{x,n}$ for the type I Lamb wave modes in (a) a traditional resonator and (b) transverse spurious resonance free resonators employing Piston mode structure by the design using IDT hammerhead.

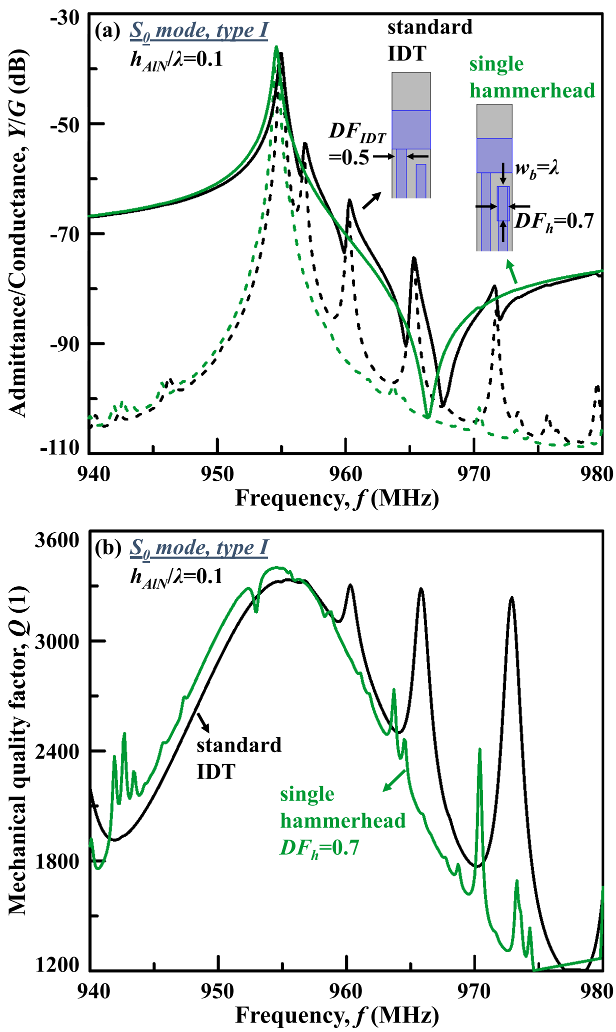

FIGURE 8. Comparison of the FEM simulated (a) frequency response and (b) mechanical Q for the S_0 mode employing conventional IDT and single hammerhead IDT with $DF_h = 0.7$ forming Piston mode structure.

lengths fits to the active region for all even modes leading to non-vanishing coupling, while for the Piston mode, the even order modes which have a multiple of full wave lengths in the active region, cancel each other and do not couple to electrical domain.

To be noted that because of the convex slowness curve of the Lamb wave modes in AlN (Fig. 5), usually the IDT dummy electrodes are not need for the energy trapping in the lateral field, which simplifies the problem [31].

There are several ways of designs to create the slow border region and thus achieve the Piston mode structure borrowed from SAW and BAW designs, including: (i) changing the duty factor of IDT electrodes at IDT ends, (ii) adding electrode metal thickness at IDT ends, (iii) adding low-velocity dielectric layer at the border region, (iv) adding high-velocity dielectric layer at the non-border active region, and (v) adding AlN mass extrudes at the sides or bottom of the AlN plate to form the border regions.

The easiest implementation of (i) consists in using larger metal coverage ratio electrode – the "hammerhead" in the border region. The proposed hammerhead IDT is shown in Fig. 7 as an example.

B. FEM DEMONSTRATION

Figs. 8, and 9 show the FEM simulated frequency response and Bode Q curves for the type I S_0 mode employing regular IDT and two types of hammerhead IDT forming the Piston mode waveguide. The optimized design yield a duty factor of the hammerhead (DF_h) of 0.7 for the single hammerhead case and a DF_h of 0.6 for the double hammerhead case. By carefully designing the metal ratio DF_h in corresponds to the slower border region phase velocity (v_b) together with the border width w_b, the relative coupling coefficients of transverse modes are reduced to a negligible level and amplitudes of the transverse modes in the type I S_0 are

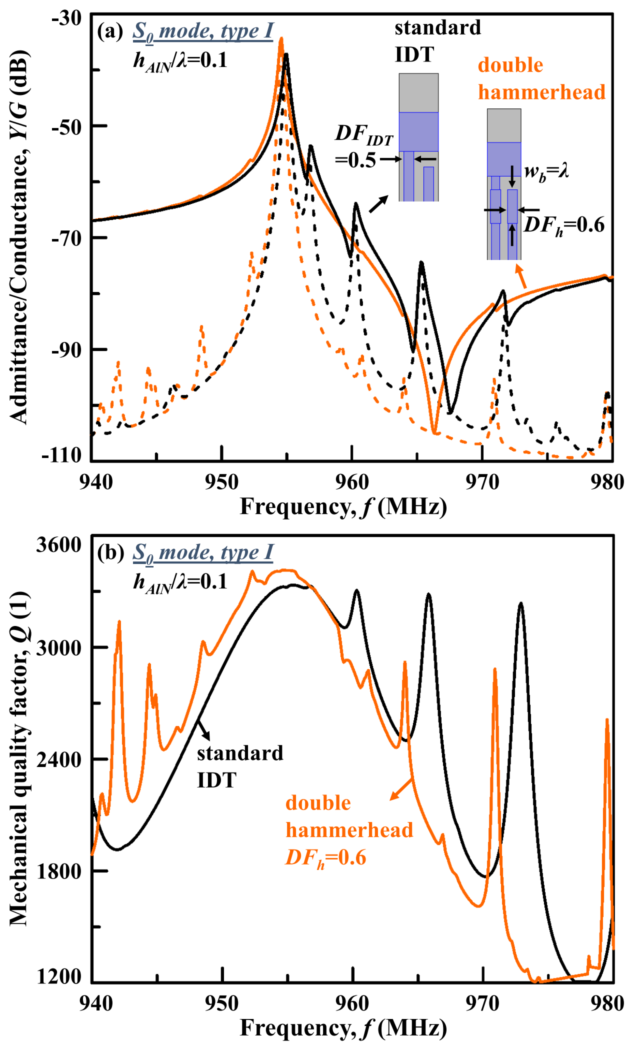

FIGURE 9. Comparison of the FEM simulated (a) frequency response and (b) mechanical Q for the S0 mode employing conventional IDT and double hammerhead IDT with $DF_h = 0.6$ forming Piston mode.

effectively reduced, or even eliminated in electrical response. In addition, the Q of the main mode is also improved by the reduction of transverse leakage, which is one of the main steps to achieve a high-Q resonator [30].

The desired border region width w_b and border region phase velocity v_b are the two main design variants for Piston mode structure. The values can be calculated by assuming small difference between the phase velocities as in [31] and fine-tuned based on the exact structure. Their relation can be written as:

$$\frac{w_b}{\lambda} \propto \frac{\Delta g}{\sqrt{\Delta b}}, \tag{8}$$

where Δb and Δg are the relative difference between the phase velocities of active region (v_a), gap region (v_g), and border region (v_b):

$$v_b = v_a(1 - \Delta b)$$
$$v_g = v_a(1 + \Delta g) \tag{9}$$

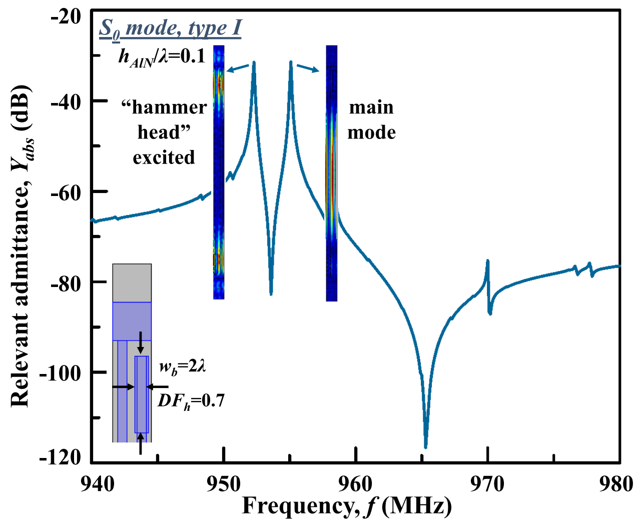

FIGURE 10. FEM simulated admittance for a Piston-mode-structure device with a border region width w_b too large.

It should be noted that the desired border region w_b/λ is not dependent on the aperture w_a/λ, rather dominated by the phase velocity differences.

Fig. 10 shows the admittance of a S0 mode resonator when the width of the border region is too large. In this case, the hammerhead no longer just works as the wave field modification region, but as the transducer itself. Thus, another resonance is excited by the hammerhead at frequency slightly lower than the main mode due to the larger duty factor, making the response split into two resonance peaks. As shown in the inset of Fig. 10, the resonance displacement of the first peak happens right at the hammerhead region and for the main mode the effective active region is reduced to $(w_a - 2w_b)$.

Similar to the S_0 mode case, this Piston mode design can be applied to other Type I Lamb wave modes for the transverse mode compensation and loss reduction.

V. CONCLUSION

For AlN Lamb wave devices, the transverse modes are strong in the large-k^2_{eff} type I modes, which deteriorate the device performance greatly by the occurrence of unwanted spurious resonances and the additional transversal loss. The dispersion characteristics for the first six Lamb wave modes are calculated: except for partial of the S_1 mode, most Lamb wave modes exhibit positive v_g and type I dispersion. By wave vector analysis and FEM simulations, the active region width w_a is found to determine the frequencies of transverse modes directly. The slowness curve indicates that the gap region guides the Lamb wave and prevents acoustic penetration into the slow busbar region, which is also demonstrated by FEM simulation. The Piston mode structure for type I Lamb wave modes created by adding a slow border region at the edge of the active aperture can eliminate the transverse modes and yet does not introduce performance degradations of the main mode. The FEM simulated AlN S_0 and type I S_1 mode

LWRs using simply hammerhead enabling the Piston mode exhibit spurious free operation. These spurious free, high Q, and large k_{eff}^2 LWRs enable the construction of single-chip filters, oscillators and sensors with superior performance characteristics.

REFERENCES

[1] V. Yantchev and I. Katardjiev, "Thin film Lamb wave resonators in frequency control and sensing applications: A review," *J. Micromech. Microeng.*, vol. 23, Apr. 2013, Art. no. 043001. doi: 10.1088/0960-1317/23/4/043001.

[2] G. Piazza, P. J. Stephanou, and A. P. Pisano, "Piezoelectric aluminum nitride vibrating contour-mode MEMS resonators," *J. Microelectromech. Syst.*, vol. 15, no. 6, pp. 1406–1418, Dec. 2006. doi: 10.1109/JMEMS.2006.886012.

[3] J. Zou, C.-M. Lin, A. Gao, and A. P. Pisano, "The multi-mode resonance in AlN Lamb wave resonators," *J. Microelectromech. Syst.*, vol. 27, no. 6, pp. 973–984, 2018. doi: 10.1109/JMEMS.2018.2867813.

[4] J. Zou *et al.*, "Low-loss, high-frequency and large-coupling SH SAW resonators based on SiN/$LiNbO_3$/Si," in *Proc. IEEE Intl. Ultrason. Symp.*, Kobe, Japan, Oct. 2018, pp. 1–4. doi: 10.1109/ULTSYM.2018.8579882.

[5] Y. Liu, Y. Bey, and X. Liu, "Extension of the hot-switching reliability of RF-MEMS switches using a series contact protection technique," *IEEE Trans. Microw. Theory Techn.*, vol. 64, no. 10, pp. 3151–3162, Oct. 2016.

[6] J. Zou and A. P. Pisano, "High-performance aluminum nitride Lamb wave resonators for RF front-end technology," Ph.D. dissertation, Univ. California, Berkeley, Berkeley, CA, USA, 2015. [Online]. Available: https://escholarship.org/uc/item/9v995545

[7] Y. Liu, Y. Bey, and X. Liu, "Single-actuator shunt-series RF-MEMS switch," in *IEEE MTT-S Int. Microw. Symp. Dig.*, Tampa, FL, USA, Jun. 2014, pp. 1–4. doi: 10.1109/MWSYM.2014.6848666.

[8] J. Zou and C. S. Lam, "Electrode design of AlN Lamb wave resonators," in *Proc. IEEE Int. Freq. Cont. Symp. (IFCS)*, New Orleans, LA, USA, May 2016, pp. 1–5. doi: 10.1109/FCS.2016.7563573.

[9] J. Zou, C.-M. Lin, C. S. Lam, and A. P. Pisano, "Transducer design for AlN Lamb wave resonators," *J. Appl. Phys.*, vol. 115, Mar. 2014, Art. no. 094510. doi: 10.1063/1.4979914.

[10] A. Anand, Y. Liu, and X. Liu, "Substrate-integrated octave-tunable combline bandstop filter with surface mount varactors," in *Proc. IEEE Int. Wireless Symp. (IWS)*, X'ian, China, Mar. 2014, pp. 1–4.

[11] Y. Liu, Y. Bey, and X. Liu, "High-power high-isolation RF-MEMS switches with enhanced hot-switching reliability using a shunt protection technique," *IEEE Trans. Microw. Theory Techn.*, vol. 65, no. 9, pp. 3188–3199, Sep. 2017.

[12] C. S. Lam, A. Gao, C.-M. Lin, and J. Zou, "A review of Lamé and Lamb mode crystal resonators for timing applications and prospects of Lamé and Lamb mode PiezoMEMS resonators for filtering applications," in *Proc. Int. Symp. Acoustic Devices Future Mobile Commun. Syst.*, Chiba, Japan, Mar. 2018, pp. 1–12.

[13] A. Gao and S. Gong, "Harnessing mode conversion for spurious mode suppression in AlN laterally vibrating resonators," *IEEE J. Microelectromech. Syst.*, vol. 25, no. 3, pp. 450–458, Jun. 2016. doi: 10.1109/JMEMS.2016.2543523.

[14] J. Zou, C.-M. Lin, and A. P. Pisano, "Quality factor enhancement in Lamb wave resonators utilizing butterfly-shaped AlN plates," in *Proc. IEEE Intl. Ultrason. Symp.*, Chicago, IL, USA, Sep. 2014, pp. 81–84. doi: 10.1109/ULTSYM.2014.0021.

[15] C.-M. Lin, V. Yantchev, J. Zou, Y.-Y. Chen, and A. P. Pisano, "Micromachined one-port aluminum nitride Lamb wave resonators utilizing the lowest-order symmetric mode," *J. Microelectromech. Syst.*, vol. 23, no. 1, pp. 78–91, Feb. 2014. doi: 10.1109/JMEMS.2013.2290793.

[16] J. Segovia-Fernandez *et al.*, "Monolithic AlN MEMS-CMOS resonant transformer for wake-up receivers," in *Proc. IEEE Int. Ultrason. Symp. (IUS)*, Washington, DC, USA, Sep. 2017, pp. 1–4.

[17] J. Zou, C.-M. Lin, Y.-Y. Chen, and A. P. Pisano, "Theoretical study of thermally stable SiO_2/AlN/SiO_2 Lamb wave resonators at high temperatures," *J. Appl. Phys.*, vol. 115, Mar. 2014, Art. no. 094510. doi: 10.1063/1.4867613.

[18] A. Gao, J. Provine, M. Winterkorn, Y. Yang, R. Lu, and S. Gong, "Boosting Qs of AlN resonators by redefining acoustic boundaries," in *Proc. IEEE 31th Int. Conf. Micro Electro Mech. Syst. (MEMS)*, Jan. 2018.

[19] J. Zou, C.-M. Lin, G. Tang, and A. P. Pisano, "High-Q butterfly-shaped AlN Lamb wave resonators," *IEEE Electron Device Lett.*, vol. 38, no. 12, pp. 1739–1742, Dec. 2017. doi: 10.1109/LED.2017.2769619.

[20] A. Gao, R. Lu, and S. Gong, "Mitigation of AO spurious modes in AlN MEMS resonators with SiO_2 addendums," in *Proc. IEEE Int. Freq. Control Symp.*, May 2016, pp. 1–5.

[21] J. Zou, C.-M. Lin, and A. P. Pisano, "Anchor loss suppression using butterfly-shaped plates for AlN Lamb wave resonators," in *Proc. IEEE Int. Freq. Control Symp.*, Denver, CO, USA, Apr. 2015, pp. 432–435. doi: 10.1109/FCS.2015.7138874.

[22] A. Gao, J. Zou, and S. Gong, "A 3.5 GHz AlN S_1 Lamb mode resonator," in *Proc. IEEE Int. Ultrason. Symp.*, Washington, DC, USA, Sep. 2017, pp. 1–4. doi: 10.1109/ULTSYM.2017.8092973.

[23] J. Zou, C.-M. Lin, Y.-Y. Chen, and A. P. Pisano, "High-frequency and low-resonance-impedance Lamb wave resonators utilizing the S_1 mode," in *Tech. Dig. Int. Conf. Solid-State Sens. Actuators Microsyst. (Transducers)*, Anchorage, AK, USA, Jun. 2015, pp. 2025–2028. doi: 10.1109/TRANSDUCERS.2015.7181353.

[24] J. Zou and A. P. Pisano, "Temperature compensation of the AlN Lamb wave resonators utilizing the S_1 mode," in *Proc. IEEE Int. Ultrason. Symp.*, Taipei, Taiwan, Oct. 2015, pp. 1–4. doi: 10.1109/ULTSYM.2015.0456.

[25] V. Yantchev and T. Mirea, "Suppression of transverse-mode spurious responses in thin film Lamb wave resonators by bandgap engineering," in *Proc. IEEE Int. Ultrason. Symp.*, Chicago, IL, USA, Sep. 2014, pp. 2552–2555. doi: 10.1109/ULTSYM.2014.0637.

[26] V. Yantchev *et al.*, "Parametric study of resonant TC-SAW piston-mode configurations," in *Proc. IEEE Int. Ultrason. Symp.*, Washington, DC, USA, Sep. 2017, pp. 1–4. doi: 10.1109/ULTSYM.2017.8091695.

[27] V. Yantchev, L. Arapan, I. Katardjiev, and V. Plessky, "Thin- film zero-group-velocity Lamb wave resonator," *Appl. Phys. Lett.*, vol. 99, Jun. 2011, Art. no. 033505. doi: 10.1063/1.3614559.

[28] Y. Liu, J. Liu, Y. Wang, and C. S. Lam, "A novel structure to suppress transverse modes in radio frequency TC-SAW resonators and filters," *IEEE Microw. Wireless Compon. Lett.*, to be published.

[29] J. Zou, J. Liu, G. Tang, C.-M. Lin, and C. S. Lam, "Transverse mode suppression in the AlN Lamb wave resonators by 'piston mode,'" in *Proc. IEEE Int. Ultrason. Symp.*, Washington, DC, USA, Sep. 2017, pp. 1–4. doi: 10.1109/ULTSYM.2017.8092899.

[30] B. Abbott *et al.*, "Temperature compensated SAW with high quality factor," in *Proc. IEEE Intl. Ultrason. Symp.*, Washington, DC, USA, Sep. 2017, pp. 1–7. doi: 10.1109/ULTSYM.2017.8092294.

[31] M. Solal *et al.*, "Transverse modes suppression and loss reduction for buried electrodes SAW devices," in *Proc. IEEE Int. Ultrason. Symp.*, San Diego, CA, USA, Oct. 2010, pp. 624–628. doi: 10.1109/ULTSYM.2010.5935738.

[32] S. A. Wilkus, C. S. Hartmann, and R. J. Kansy, "Transverse mode compensation of surface acoustic wave filters," in *Proc. IEEE Int. Ultrason. Symp.*, San Francisco, CA, USA, Oct. 1985, pp. 43–47. doi: 10.1109/ULTSYM.1985.198475.

[33] H. Nakamura *et al.*, "Suppression of transverse mode spurious in SAW resonators on an SiO_2/Al/$LiNbO_3$ Structure for wideband CDMA applications," in *Proc. IEEE Int. Ultrason. Symp.*, Beijing, China, Nov. 2008, pp. 594–597. doi: 10.1109/ULTSYM.2008.0142.

[34] J. Kaitila, M. Ylilammi, J. Ellä, and R. Aigner, "Spurious resonance free Bulk acoustic wave resonators," in *Proc. IEEE Int. Ultrason. Symp.*, Honolulu, HI, USA, Oct. 2003, pp. 84–87. doi: 10.1109/ULTSYM.2003.1293361.

[35] R. Thalhammer, J. Kaitila, S. Zieglmeier, and L. Elbrecht, "4E-3 spurious mode suppression in BAW resonators," in *Proc. IEEE Int. Ultrason. Symp.*, Vancouver, BC, Canada, Oct. 2006, pp. 456–459. doi: 10.1109/ULTSYM.2006.122.

[36] R. Ruby, J. Larson, C. Feng, and S. Fazzio, "The effect of perimeter geometry on FBAR resonator electrical performance," in *IEEE MTT-S Int. Microw. Symp. Dig.*, Jul. 2005, pp. 217–221. doi: 10.1109/MWSYM.2005.1516563.

[37] G. G. Fattinger, S. Marksteiner, J. Kaitila, and R. Aigner, "Optimization of acoustic dispersion for high performance thin film BAW resonators," in *Proc. IEEE Int. Ultrason. Symp.*, Rotterdam, The Netherlands, Sep. 2005, pp. 1175–1178. doi: 10.1109/ULTSYM.2005.1603060.

[38] J. Liu, T. Omori, C. Ahn, and K.-Y. Hashimoto, ''Impact of surface periodic grating on FBAR structures to spurious transverse resonances,'' in *Proc. IEEE Int. Ultrason. Symp.*, Prague, Czech Republic, Jul. 2013, pp. 1957–1960. doi: 10.1109/ULTSYM.2013.0499.

[39] J. Liu, T. Omori, C. Ahn, and K.-Y. Hashimoto, ''Design and simulation of coupled-resonator filters using periodically slotted electrodes on FBARs [Correspondence],'' *IEEE Trans. Ultrason., Ferroelectr., Freq. Control*, vol. 61, no. 5, pp. 881–885, May 2014.

[40] B. Zhang *et al.*, ''Impact of coupling between multiple SAW modes on Piston mode operation of SAW resonators,'' in *Proc. IEEE Intl. Ultrason. Symp.*, Washington, DC, USA, Sep. 2017, pp. 1–4. doi: 10.1109/ULTSYM.2017.8091961.

[41] K. Hashimoto, H. Asano, K. Matsuda, N. Yokoyama, T. Omori, and M. Yamaguchi, ''Wideband love wave filters operating in GHz range on Cu-grating/rotated-YX-$LiNbO_3$-substrate structure,'' in *Proc. IEEE Int. Ultrason. Symp.*, Montreal, QC, Canada, Aug. 2004, pp. 1330–1334. doi: 10.1109/ULTSYM.2004.1418039.

[42] H. Zhang, J. Liang, H. Zhang, D. Zhang, and W. Pang, ''Spurious-free Lamb wave resonators with protrusion structures,'' *Appl. Phys. Lett.*, vol. 107, Dec. 2015, Art. no. 243502. doi: 10.1063/1.4937736.

[43] H. Zhang, J. Liang, X. Zhou, H. Zhang, D. Zhang, and W. Pang, ''Transverse mode spurious resonance suppression in Lamb wave MEMS resonators: Theory, modeling, and experiment,'' *IEEE Trans. Electron Devices*, vol. 62, no. 9, pp. 3034–3041, Sep. 2015. doi: 10.1109/TED.2015.2458913.

[44] W. J. Tanski and N. D. Wittels, ''SEM observations of SAW resonator transverse modes,'' *Appl. Phys. Lett.*, vol. 34, p. 537, Feb. 1979. doi: 10.1063/1.90878.

[45] M. Giovannini, S. Yazici, N.-K. Kuo, and G. Piazza, ''Apodization technique for spurious mode suppression in AlN contour-mode resonators,'' *Sens. Actuators A, Phys.*, vol. 206, pp. 42–50, Dec. 2013. doi: 10.1016/j.sna.2013.11.023.

[46] C. K. Campbell, P. J. Edmonson, and P. M. Smith, ''Transverse modes in one-port SAW resonators,'' *IEEE Trans. Ultrason., Ferroelectr., Freq. Control*, vol. 39, no. 6, pp. 785–787, Nov. 1992. doi: 10.1109/58.165565.

[47] K. Hashimoto, *Surface Acoustic Wave Devices in Telecommunications: Modelling and Simulation*. Berlin, Germany: Springer-Verlag, 2000.

JIE ZOU received the Ph.D. degree in mechanical engineering and the M.S. degree in electrical engineering from the University of California, Berkeley, CA, USA, in 2015 and 2014, respectively. From 2015 to 2018, she was a Senior Acoustic Filter Design Engineer with the Skyworks Solutions, Inc. Irvine, CA, where she developed the TCSAW filter and duplexer products and researched on the next-generation acoustic wave devices. She is currently a Member of Technical Staff at Resonant Inc., Santa Barbara, CA. Her research interests include RF MEMS, micro-acoustic resonators, piezoelectric resonators and filters, and telecommunication front-end technologies.

JIANSONG LIU received the Ph.D. degree in electronics engineering from Chiba University, Japan, in 2014. Thereafter, he was with Taiyo Yuden Co. Ltd., where he was involved in the Research and Development of FBAR devices. Since 2017, he has been with Skyworks Solutions Inc., where he currently develops high performance FBAR filter technology. His research interests include simulation and design of various high-performance FBAR/BAW/SAW devices, lamb wave devices, and RF circuit designs.

GONGBIN TANG was born in 1987. He received the Dr.Eng. degree in instrument engineering from Shanghai Jiao Tong University and the Ph.D. degree in electronics engineering from Chiba University. He is currently a Research Engineer with Skyworks Solutions, Japan. His research interests include simulation and design of various high-performance surface acoustic wave devices, piezoelectric materials, and RF circuit designs.